Yrast-yrare interaction strength and bandcrossing frequency

C. S. Wu and J. Y. Zeng*
China Center of Advanced Science and Technology (World Laboratory), Center of Theoretical Physics, P.O. Box 8730, Beijing 100080, China;
Department of Physics, Peking University, Beijing 100871, China;
and Institute of Theoretical Physics, Chinese Academy of Science, Beijing 100080, China
(Received 16 May 1991)

Accurate particle-number-conserving calculation shows that in a single-j model the yrast-yrare interaction V is always strong and no periodic oscillation of V with the degree of shell filling is found, in contrast to the results obtained by the Hartree-Fock-Bogoliubov approximation. To understand the behavior of V and bandcrossing frequency ω_c, the spin-alignment, seniority structure, configuration structure, and "quasiparticle structure" of the yrast and yrare bands are analyzed in detail. Calculation in a two-j model (high-j intruder orbits plus normal orbits of opposite parity) was also carried out to illustrate schematically that a weak yrast-yrare interaction may occur for certain single-particle level scheme. The coexistence of normal low-j orbits with high-j intruder orbits is indispensible for a sharp backbending observed in some realistic nuclei.

I. INTRODUCTION

It is well known that the sharpness of the first backbending in nuclear yrast spectra depends on the magnitude of the interaction strength between the yrast and yrare bands. A famous conclusion was drawn in Ref. [1] that in the Hartree-Fock-Bogoliubov (HFB) calculation for a single-j ($i\frac{13}{2}$) cranked shell model (CSM) [2,3] the yrast-yrare interaction strength, V, is a periodic function of the degree of shell filling and thus a sharp backbending may be expected not only at the bottom of the neutron $i\frac{13}{2}$ shell, but also may be obtained for appropriate configurations even near the top of the shell. This striking feature has attracted much attention of may nuclear physicists [4–7].

General considerations show that the Bardeen-Cooper-Schrieffer (BCS) or HFB approximation is very suitable for a system of a large number of particles. The question is, however, how reliable is the HFB approximation for treating the eigenvalue problem of nuclear CSM Hamiltonian [8]. The crucial problem is that the number of nucleons in a nucleus ($\sim 10^2$), particularly, the number of valence nucleons (~ 10) which dominate the behavior of nuclear low-lying states, is very limited. As a result, the nonconservation of particle number may lead to serious consequences [8,9]. Therefore, one has to be very careful in drawing conclusions from the HFB approximation. For example, in all self-consistent solutions to the cranked HFB equations a pairing collapse has been found [10–12], but calculations with particle-number projection before variation show that the gap parameter decreases very slowly and no sharp phase transition is found [8]. It was also emphasized [2] that the calculated results, in general, may not be reliable when the cranked HFB theory is applied to the bandhead and the bandcrossing regions. However, just the behaviors of the yrast and yrare bands in the bandcrossing region determine the yrast-yrare interaction. Therefore, conclusions concerning the yrast-yrare interaction and bandcrossing frequency drawn from the HFB treatment for the CSM seems questionable.

As usual, the CSM Hamiltonian of an axially symmetric nucleus in the rotating frame is expressed as [13]

$$H_{\rm CSM}=H_{\rm intr}+H_C=H_{sp}+H_P+H_C\ , \tag{1}$$

$$H_{sp}=\sum_\nu \varepsilon_\nu a_\nu^\dagger a_\nu\ , \tag{2}$$

$$H_P=-G\mathbf{P}^\dagger\mathbf{P},\quad \mathbf{P}=\sum_{\mu>0} a_{\bar\mu}a_\mu\ , \tag{3}$$

$$H_C=-\omega J_x=-\omega\sum_{\mu\nu}\langle\mu|j_x|\nu\rangle a_\mu^\dagger a_\nu\ , \tag{4}$$

where H_{sp} is the single-particle Hamiltonian, $\mathbf{H}_P$ the pairing interaction with a constant strength G, and H_C the Coriolis interaction with cranking frequency ω about x axis perpendicular to the symmetry z axis (for details, see Ref. [13]).

In the HFB approximation (mean field approximation) $H_{\rm intr}$ is replaced by [13]

$$H'_{\rm intr}=\sum_\nu(\varepsilon_\nu-\lambda)a_\nu^\dagger a_\nu-\frac{\Delta}{2}(\mathbf{P}^\dagger+\mathbf{P})\ , \tag{5}$$

where λ is the Fermi energy and $\Delta=G\langle\mathbf{P}\rangle$ is the gap parameter. However, it is very difficult to justify such a replacement theoretically. In the mean field approximation the residual quasiparticle interactions are completely ignored. The residual quasiparticle interactions may come from two sources. One is the usually ignored higher-order terms containing four-quasiparticle creation and/or annihilation operators in the pairing Hamiltonian [14,15], which are very complicated to be taken into account even in the perturbation theory. The other one is the blocking effect. Calculation shows that the blocking effects, espe-

cially the blocking of the single-particle levels near the Fermi surface, are very important for the low-lying eigenstates [16]. Various even-odd differences (mass or binding energy, energy gap, moment of inertia, two-nucleon transfer reaction, bandcrossing frequency, etc.) are essentially attributed to the blocking effects. As pointed out by Rowe [17], however, while the blocking effects are straightforward, it is very difficult to treat them in the BCS or HFB formalism because different quasiparticle bases are introduced for different blocked levels.

It was shown [18,19] that the accurate solutions to the low-lying eigenstates of CSM Hamiltonian may be obtained easily by the particle-number-conserving (PNC) treatment, in which a many-particle configuration (MPC) truncation is adopted instead of the usual single-particle level (SPL) truncation. The advantage of the MPC truncation over the SPL truncation has been demonstrated thoroughly in Ref. [20]. A very useful representation of the MPC space, which was introduced in Ref. [19], is adopted in this paper. In this representation each of the many-particle basis states are characterized by N (particle number of the system), π (parity), r (signature), v (seniority), K (K^2 being the eigenvalue of J_z^2), and E_i (configuration energy, the sum of all the occupied single-particle energies). Here it should be emphasized that the quantum number K (≥ 0) is a label to specify the eigenvalue of J_z^2 (but not J_z). To avoid repetition the PNC formalism of the CSM calculation in this representation space is omitted in this paper. We refer the reader to Ref. [19] for details.

In this paper the PNC formalism is used to investigate the yrast-yrare interaction and the bandcrossing frequency for even N systems. Therefore we restrict ourselves to the configuration space of $\pi=+$ and $r=1$. As usual, the bandcrossing frequency ω_c is defined as

$$(\langle J_x \rangle_{\text{yrare}} - \langle J_x \rangle_{\text{yrast}})_{\omega=\omega_c} = 0 \tag{6}$$

and the yrast-yrare interaction V is known as one-half of the minimal separation between the yrast and yrare bands,

$$\begin{aligned} V &= \tfrac{1}{2}(E_{\text{yrare}} - E_{\text{yrast}})_{\min} \\ &= \tfrac{1}{2}(E_{\text{yrare}} - E_{\text{yrast}})_{\omega=\omega_c} . \end{aligned} \tag{7}$$

In Sec. II calculation in a single-j ($j=\frac{13}{2}$) model is carried out to show how the yrast-yrare interaction V and bandcrossing frequency ω_c vary with the degree of shell filling. To understand microscopically the behavior of V and ω_c, the spin-alignment, seniority structure, K structure, configuration structure, and "quasiparticle structure" are discussed in detail. Calculation definitely shows that no weak yrast-yrare interaction is found in the single-j model. As an improvement on the single-j model, calculation in a schematic two-j model ($j^\pi=\frac{13}{2}^+$ plus $i^\pi=\frac{7}{2}^-$) is given in Sec. III. It is found that for certain single-particle level distribution in the two-j model, weak yrast-yrare interactions do occur. A brief summary is given in Sec. IV.

II. YRAST-YRARE INTERACTION AND BANDCROSSING FREQUENCY IN A SINGLE-j MODEL

As in Ref. [1], calculation in a single-j CSM ($j=\frac{13}{2}$) was carried out to illustrate how the yrast-yrare interaction strength and the first bandcrossing frequency vary with the Fermi energy. The single-particle energy is assumed to be [2,3]

$$\varepsilon_{|\Omega|} = \kappa \frac{3\Omega^2 - j(j+1)}{j(j+1)} + e_0, \quad |\Omega| = \tfrac{1}{2}, \tfrac{3}{2}, \ldots, j . \tag{8}$$

The accurate solutions to the low-lying eigenstates of H_{CSM} are obtained by the PNC method [18,19] with MPC truncation [20]. We diagonalize H_{CSM} in a large truncated configuration space with $E_c = 3.5\kappa \sim 10$ MeV. This means that all the many-particle configurations (including seniority $v=0,2,4,6,\ldots$) with energies $(E - E_0) \leq E_c$ are taken into account, where E_0 is the energy of the lowest configuration. Calculation in the full (untruncated) MPC space has been also carried out to judge the degree of accuracy of the MPC truncation. The results show that the solutions obtained in the MPC truncation are accurate enough (see Ref. [21], and also Fig. 2 below). In fact, all the non-negligible configurations (weight $\geq 10^{-3}$) have been involved in the MPC truncation (see Tables I and II), while almost all the main configurations (weight $\geq 10^{-2}$) are relatively low ($E - E_0 < 2.0\kappa$). The pairing interaction strength is reasonably but somewhat arbitrarily chosen as $G/\kappa = 0.15$. Calculation shows that the conclusions drawn below remain valid for other G values within a reasonable region.

In the PNC calculation the Fermi energy λ is defined as follows: For the yrast state (at $\omega=0$) of a given system the occupation probability of a single-particle level at the Fermi surface by a pair of particles is 50%. The $\lambda(N)$'s for various N-particle systems are shown in Fig. 1. Calculations show that the value of λ is very insensitive to the magnitude of pairing interaction strength G. In fact,

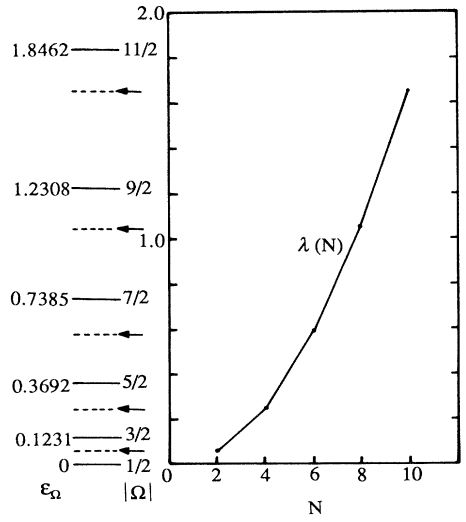

FIG. 1. $\lambda(N)$ vs N plot in a single j ($j=\frac{13}{2}$). $E_c/\kappa = 3.5$. For each N, the calculated $\lambda(N)$'s for $G/\kappa = 0.10$, 0.15, and 0.20 are so close that they are hard to be distinguished with each other in the plot.

TABLE I. The non-negligible configurations (weight $\geq 10^{-3}$) for the yrast band of an eight-particle system in the single-j model ($j=\frac{13}{2}$). The first column gives the configurations. The second and third columns list the K values and the configuration energies (in units of κ), respectively. The fourth through ninth column list the amplitudes of each configurations in the yrast band. The main configurations (weight $\geq 1\%$) are marked by asterisks. In the first column, 1234 means that the single-particle levels 1, 2, 3, and 4 are each occupied by a pair of particles; $123(\bar{4}\bar{5})$ represents a pair-broken configuration, in which three pairs of particles occupy the single-particle levels 1, 2, and 3, and the remaining two unpaired particles block the single-particle levels 4 and 5 with resultant $K=|\Omega_5-\Omega_4|$; $12(\bar{3}\,\bar{4}56)$ denotes a $v=4$ configuration in which the four unpaired particles block the single-particle levels 3, 4, 5, and 6 with $K=|\Omega_5+\Omega_6-\Omega_3-\Omega_4|$ and the other two pairs of particles occupy the single-particle levels 1 and 2; etc.

Configurations	K	Configuration energies (κ)	Amplitude in yrast band (0_1^+) $\omega/\kappa=0$	0.04	0.08	0.12	0.16	0.20
1234	0	0.0000	0.9627 *	0.9228 *	0.8118 *	0.6537 *	0.4822 *	0.3326 *
1235	0	0.9846	0.1830 *	0.2134 *	0.2868 *	0.3600*	0.3905 *	0.3671 *
1236	0	2.2154	0.0813	0.0811	0.0826	0.0884	0.0968	0.1018 *
1245	0	1.7231	0.1129 *	0.1154 *	0.1276 *	0.1559 *	0.1941 *	0.2235*
1246	0	2.9538	0.0593	0.0586	0.0578	0.0610	0.0718	0.0880
1345	0	2.2154	0.0898	0.0903	0.0918	0.0964	0.1064 *	0.1200 *
1346	0	3.4462	0.0504	0.0487	0.0444	0.0400	0.0390	0.0424
2345	0	2.4615	0.0789	0.0782	0.0760	0.0725	0.0683	0.0646
$123(\bar{4}\bar{5})$	1	0.4923		−0.2414 *	−0.4204 *	−0.4979 *	−0.4741 *	−0.3898 *
$125(\bar{3}\bar{4})$	1	1.3538		−0.0394	−0.1054 *	−0.1971 *	−0.2822 *	−0.3255 *
$126(\bar{3}\bar{4})$	1	2.5846				−0.0456	−0.0739	−0.1017 *
$123(\bar{5}6)$	1	1.6000			−0.0669	−0.1249 *	−0.1790 *	−0.2071 *
$124(\bar{5}6)$	1	2.3385				−0.0591	−0.1046 *	−0.1529 *
$134(\bar{5}6)$	1	2.8308					−0.0515	−0.0769
$234(\bar{5}6)$	1	3.0769						−0.0334
$145(\bar{2}3)$	1	1.9692			−0.0397	−0.0718	−0.1175 *	−0.1651 *
$146(\bar{2}3)$	1	3.2000					−0.0379	−0.0594
$345(\bar{1}2)$	1	2.3385				−0.0379	−0.0534	−0.0718
$124(\bar{3}5)$	2	0.8615			0.1072 *	0.1897 *	0.2388 *	0.2413 *
$123(\bar{4}6)$	2	1.1077			−0.0667	−0.1178 *	−0.1478 *	−0.1488 *
$125(\bar{4}6)$	2	2.8308						0.0323
$135(\bar{2}4)$	2	1.6000				0.0648	0.1229 *	0.1744 *
$136(\bar{2}4)$	2	2.8308					0.0318	0.0547
$245(\bar{1}3)$	2	2.0923					0.0456	0.0780
$123(\bar{5}7)$	2	2.3385						−0.0351
$134(\bar{2}5)$	3	1.1077				−0.0622	−0.1043 *	−0.1303 *
$124(\bar{3}6)$	3	1.4769				0.0631	0.1056 *	0.1322 *
$125(\bar{3}6)$	3	2.4615						0.0482
$235(\bar{1}4)$	3	1.7231					−0.0500	−0.0870
245(13)	3	2.0923						0.0338
$234(\bar{1}5)$	4	1.2308					0.0431	0.0665
235(14)	4	1.7231						−0.0424
$134(\bar{2}6)$	4	1.7231					−0.0534	−0.0825
$135(\bar{2}6)$	4	2.7077						−0.0381
234(15)	5	1.2308						0.0339
$234(\bar{1}6)$	5	1.8462						0.0450
$12(3\bar{4}\,\bar{5}6)$	0	1.9692				−0.0526	−0.0966	−0.1342 *
$14(2\bar{3}\,\bar{5}6)$	0	2.5846					−0.0476	−0.0816
$34(1\bar{2}\,\bar{5}6)$	0	2.9538						−0.0317
$13(\bar{2}45\bar{6})$	1	2.2154					0.0428	0.0720
$24(\bar{1}35\bar{6})$	1	2.7077						0.0381
$12(\bar{3}4\bar{5}6)$	2	1.9692				0.0626	0.1187 *	0.1684 *
$23(\bar{1}45\bar{6})$	2	2.3385						−0.0335
$14(\bar{2}\bar{3}56)$	2	2.5846					0.0502	0.0876
$34(\bar{1}\bar{2}56)$	2	2.9538						0.0326
$13(\bar{2}4\bar{5}6)$	3	2.2154					−0.0577	−0.1002 *
$24(\bar{1}3\bar{5}6)$	3	2.7077						−0.0428
$12(\bar{3}\,\bar{4}56)$	4	1.9692						−0.0342
$23(\bar{1}\bar{4}56)$	4	2.3385						0.0525

TABLE II. The same as Table I for the yrare band.

Configurations	K	Configuration energies (κ)	$\omega/\kappa=0$	Amplitude in yrare band 0.04	0.08	0.12	0.16	0.20
1234	0	0.0000		0.2942 *	0.3668 *	0.3564 *	0.2955*	0.2434 *
1235	0	0.9846		−0.2765 *	−0.2699 *	−0.1260 *	0.0422	0.1477 *
1245	0	1.7231			−0.0623	−0.1095 *	−0.0873	
1345	0	2.2154					−0.0491	−0.0457
123($\bar{4}$5)	1	0.4923	0.9987 *	0.8067 *	0.2965 *	−0.0378	−0.2020 *	−0.2527 *
126($\bar{4}$5)	1	3.4462	0.0506	0.0384				
125($\bar{3}$4)	1	1.3538		0.0986	0.2156 *	0.2278 *	0.1125 *	
126($\bar{3}$4)	1	2.5846				0.0436	0.0385	
123($\bar{5}$6)	1	1.6000		0.0503	0.1062 *	0.0999		−0.0450
124($\bar{5}$6)	1	2.3385				0.0743	0.0818	0.0486
134($\bar{5}$6)	1	2.8308					0.0474	0.0504
145($\bar{2}$3)	1	1.9692			0.0328	0.0989	0.1278 *	0.1039 *
146($\bar{2}$3)	1	3.2000					0.0362	0.0379
345($\bar{1}$2)	1	2.3385					0.0511	0.0617
124($\bar{3}$5)	2	0.8615		−0.2965 *	−0.3081 *	−0.1949 *	−0.0438	0.0529
123($\bar{4}$6)	2	1.1077		0.1373 *	0.1302 *	0.0563		−0.0715
135($\bar{2}$4)	2	1.6000			−0.0927	−0.1821 *	−0.1819 *	−0.1259 *
136($\bar{2}$4)	2	2.8308				−0.0344	−0.0495	−0.0460
245($\bar{1}$3)	2	2.0923				−0.0666	−0.1172 *	−0.1318 *
246($\bar{1}$3)	2	3.3231					−0.0321	−0.0439
345(12)	2	2.3385					0.0338	0.0461
134($\bar{2}$5)	3	1.1077		0.0667	0.1613 *	0.2131 *	0.1630 *	0.0947
124($\bar{3}$6)	3	1.4769		−0.0481	−0.1051 *	−0.1141 *	−0.0643	
125($\bar{3}$6)	3	2.4615				−0.0321	−0.0354	
235($\bar{1}$4)	3	1.7231			0.0434	0.1426 *	0.1998 *	0.1989 *
236($\bar{1}$4)	3	2.9538					0.0501	0.0635
245(13)	3	2.0923				−0.0540	−0.1043 *	−0.1317 *
246(13)	3	3.3231						−0.0435
234($\bar{1}$5)	4	1.2308			−0.0859	−0.1917 *	−0.2084 *	−0.1778 *
235(14)	4	1.7231			0.0374	0.1358 *	0.2063 *	0.2284 *
236(14)	4	2.9538					0.0495	0.0699
134($\bar{2}$6)	4	1.7231			0.0531	0.1084 *	0.1158 *	0.0922
135($\bar{2}$6)	4	2.7077					0.0501	0.0549
145(23)	4	1.9692				0.0447	0.0767	0.0950
146(23)	4	3.2000						0.0324
234(15)	5	1.2308			−0.0858	−0.2037 *	−0.2363 *	−0.2216 *
135(24)	5	1.6000			−0.0613	−0.1534 *	−0.2026 *	−0.2174 *
136(24)	5	2.8308					−0.0465	−0.0645
234($\bar{1}$6)	5	1.8462				−0.0937	−0.1359 *	−0.1439 *
235($\bar{1}$6)	5	2.8308					−0.0520	−0.0718
134(25)	6	1.1077			0.1657 *	0.2649 *	0.2627 *	0.2363 *
125(34)	6	1.3538			0.0954	0.1474 *	0.1509 *	0.1441 *
126(34)	6	2.5846					0.0321	0.0406
234(16)	6	1.8462				−0.0987	−0.1517 *	−0.1746 *
235(16)	6	2.8308					−0.0545	−0.0819
234($\bar{1}$7)	6	2.5846						−0.0336
124(35)	7	0.8615		−0.0763	−0.3483 *	−0.3436 *	−0.2611 *	−0.2071 *
134(26)	7	1.7231			0.0535	0.1288 *	0.1696 *	0.1874 *
135(26)	7	2.7077					0.0577	0.0841
234(17)	7	2.5846						−0.0407
123(45)	8	0.4923		0.2213 *	0.4924 *	0.3058 *	0.1723 *	0.1151 *
124(36)	8	1.4769			−0.1119 *	−0.1662 *	−0.1681 *	−0.1644 *
125(36)	8	2.4615					−0.0452	−0.0594
134(27)	8	2.4615					0.0346	0.0458
123(46)	9	1.1077		0.0357	0.1587 *	0.1474 *	0.1097 *	0.0899
124(37)	9	2.2154					−0.0352	−0.0417
123(56)	10	1.6000			0.0337	0.0474	0.0474	0.0481
124(56)	10	2.3385						0.0344

TABLE II. (*Continued*).

Configurations	K	Configuration energies (κ)	Amplitude in yrare band $\omega/\kappa=0$	0.04	0.08	0.12	0.16	0.20
12($3\bar{4}\,\bar{5}6$)	0	1.9692			0.0464	0.0767	0.0581	
14($2\bar{3}\,\bar{5}6$)	0	2.5846				0.0383	0.0626	0.0608
34($1\bar{2}\,\bar{5}6$)	0	2.9538						0.0341
13($\bar{2}45\bar{6}$)	1	2.2154				−0.0513	−0.0665	−0.0551
24($\bar{1}35\bar{6}$)	1	2.7077					−0.0502	−0.0653
12($\bar{3}45\bar{6}$)	2	1.9692			−0.0626	−0.1057 *	−0.0851	
23($\bar{1}45\bar{6}$)	2	2.3385				0.0365	0.0657	0.0768
14($\bar{2}35\bar{6}$)	2	2.5846				−0.0440	−0.0737	−0.0750
24($135\bar{6}$)	2	2.7077					−0.0416	−0.0613
34($\bar{1}25\bar{6}$)	2	2.9538						−0.0391
13($\bar{2}45\bar{6}$)	3	2.2154				0.0816	0.1105 *	0.1003 *
23($145\bar{6}$)	3	2.3385				0.0325	0.0640	0.0837
14($235\bar{6}$)	3	2.5846						0.0422
24($\bar{1}35\bar{6}$)	3	2.7077					0.0645	0.0872
15($\bar{2}34\bar{6}$)	3	3.0769						0.0327
13($\bar{2}45\bar{6}$)	4	2.2154				−0.0340	−0.0591	−0.0756
23($\bar{1}45\bar{6}$)	4	2.3385				−0.0631	−0.1162 *	−0.1416 *
24($135\bar{6}$)	4	2.7077					0.0571	0.0864
25($\bar{1}34\bar{6}$)	4	3.2000						−0.0347
12($\bar{3}45\bar{6}$)	5	1.9692					0.0396	0.0455
13($\bar{2}\,\bar{4}56$)	5	2.2154					−0.0441	−0.0455
23($145\bar{6}$)	5	2.3385				−0.0602	−0.1195 *	−0.1605 *
14($235\bar{6}$)	5	2.5846					−0.0430	−0.0641
25($134\bar{6}$)	5	3.2000						−0.0349
13($245\bar{6}$)	6	2.2154				0.0688	0.1190 *	0.1553 *
23($\bar{1}\,\bar{4}56$)	6	2.3385					0.0508	0.0655
12($34\bar{5}6$)	7	1.9692				−0.0668	−0.0901	−0.1052 *
23($1\bar{4}56$)	7	2.3385					0.0567	0.0789
13($24\bar{5}7$)	7	2.9538						0.0335
13($2\bar{4}56$)	8	2.2154				−0.0374	−0.0644	−0.0862
12($3\bar{4}56$)	9	1.9692				0.0493	0.0657	0.0784
14($2\bar{3}56$)	9	2.5846						0.0335

the λ values obtained for $G/\kappa=0.10$, 0.15, and 0.20 are too close to be distinguished with each other in the plot. Thus, in the PNC treatment, once the particle number N is given, the Fermi energy λ is fixed in fact. This situation is quite different from that in the HFB approximation.

The calculated yrast-yrare interaction and bandcrossing frequency for $N=2,4,6,8$, and 10 particle systems are shown in Fig. 2. Observation of Fig. 2 shows the following. (1) The yrast-yrare interaction V is always rather strong for various N particle systems. (2) V increases monotonically with increasing N (or λ), and no periodic oscillation with the degree of shell filling is found. (3) The bandcrossing frequency ω_c increases almost linearly with increasing N (or λ). These results are easily understandable from the properties of the yrast and yrare bands. As an illustrative example, the detailed features of the yrast and yrare bands for an eight-particle system are discussed below. The spin-alignments ($\langle J_x\rangle_{\text{yrast}}$ and $\langle J_x\rangle_{\text{yrare}}$), the seniority structure, and the K structure are shown in Figs. 3, 4, 5, respectively. To demonstrate these results microscopically, the distribution of low-lying configurations (i.e., eigenstates of H_{sp}) for the eight-particle system is shown in Fig. 6(a). It is seen that there exist many fully paired ($v=0$) $K=0$ configurations. For the eight-particle system the lowest $K=0$ configuration is 1234, which means that the single-particle levels 1, 2, 3, and 4 are each occupied by a pair of particles, where the single-particle levels $\Omega=\frac{1}{2}, \frac{3}{2}, \ldots, \frac{13}{2}$ are labeled by $1,2,\ldots,7$, respectively. (Here we adopt an abbreviated notation for the configuration as used in Ref. [19].) It is also seen that there exist many pair-broken ($v=2$) configurations. The lowest $v=2$ configurations for the eight-particle system are $123(\bar{4}5)K^{\pi}=1^{+}$ and $123(45)K^{\pi}=8^{+}$, in which the single-particle levels 1, 2, and 3 are each occupied by a pair of particles and the single-particle levels 4 ($|\Omega|=\frac{7}{2}$) and 5 ($|\Omega|=\frac{9}{2}$) are blocked by two unpaired particles with resultant $K=|\frac{9}{2}\pm\frac{7}{2}|=1$ and 8, respectively.

In the single-j model there are always many pair-broken (seniority $v=2$) $K^{\pi}=1^{+}$ configurations, which are strongly coupled with the fully paired $K^{\pi}=0^{+}$ configurations by the Coriolis interaction. For example, for the eight-particle system, the lowest $v=2$ configuration $123(\bar{4}5)K^{\pi}=1^{+}$ is strongly coupled with the configurations 1234 and 1235 due to a very large j_x matrix element between the high-j single-particle states 4 ($|\Omega|=\frac{7}{2}$) and 5 ($|\Omega|=\frac{9}{2}$),

$$\langle 123(\bar{4}5)|j_x|1234\rangle = \langle 123(\bar{4}5)|j_x|1235\rangle = -\sqrt{2}\langle \Omega=\tfrac{7}{2}|j_x|\Omega=\tfrac{9}{2}\rangle = -\sqrt{16.5} \quad \text{for } j=\tfrac{13}{2} .$$

Similarly, the low-lying configuration $125(\bar{3}4)K^\pi=1^+$ is strongly coupled with the configurations 1235 and 1245, the low-lying configuration $123(\bar{5}6)K^\pi=1^+$ is strongly coupled with the configurations 1235 and 1236, $145(\bar{2}3)K^\pi=1^+$ is strongly coupled with 1245 and 1345, etc.

Needless to say, the angular momentum alignment along the rotating x axis, $\langle J_x\rangle$, for an eigenstate of J_z^2 of an even N system is strictly zero. However, when the Coriolis interaction is switched on ($\omega\neq 0$), v and K no longer remain good quantum numbers. The pair-broken ($v=2$) configurations, particularly, the $K^\pi=1^+$ configurations, will be gradually mixed with the $K^\pi=0^+$ configurations resulting in a large spin alignment. In fact, for a given N system the distribution of the low-lying pair-broken $K^\pi=1^+$ configurations determines the magnitude of spin-alignment $\langle J_x\rangle_{\text{yrast}}$ in low-ω region, hence the moment of inertia $\mathcal{J}_{\text{yrast}}=\langle J_x\rangle_{\text{yrast}}/\omega$ near the bandhead [22].

To display separately the influence of the pairing interaction and the Coriolis interaction on the intrinsic structure of CSM wave function, let us at the first step diagonalize the intrinsic Hamiltonian

$$H_{\text{intr}}=H_{sp}+H_P=H_{\text{CSM}}(\omega=0) . \tag{9}$$

In this case, v and K are still good quantum numbers for a well-deformed nucleus and the eigenstate may be denoted by $(\nu_1\nu_2\cdots\nu_{2k})K_i^\pi$ which refers to the ith K^π eigenstate with blocked levels $\nu_1,\nu_2,\ldots,\nu_{2k}$. The low-lying eigenstates of H_{intr} ("quasiparticle spectrum") for the eight-particle system are shown in Fig. 6(b). The non-negligible configurations (with weight $\geq 10^{-3}$) and the corresponding amplitudes in the two lowest eigenstates of H_{intr} are listed in the fourth column of Tables I and II. The lowest (yrast) state 0_1^+ is a coherent superposition of many fully paired (seniority $v=0$) $K=0$ configurations. As a result, a large binding energy gain is obtained, hence appears an energy gap between the yrast state and the excited states. The most important configurations (weight $\geq 10\%$) in the yrast state are the three lowest configurations 1234, 1235, and 1245 (see the fourth column of Table I). The lowest excited state is pair-broken state $(\bar{4}5)1_1^+$, a superposition of many pair-broken $(v=2)K^\pi=1^+$ configurations, such as $123(\bar{4}5)$, $126(\bar{4}5)$, etc., in all these configurations the unpaired particles block the single-particle levels 4 ($|\Omega|=\frac{7}{2}$) and 5 ($|\Omega|=\frac{9}{2}$) with resultant $K=|\frac{9}{2}-\frac{7}{2}|=1$. Usually, the yrast state of an even N system is referred to as quasiparticle vacuum, while the pair-broken eigenstates of H_{intr} are considered as two quasiparticle states.

When the Coriolis interaction is switched on ($\omega\neq 0$), the eigenstates of H_{intr} will be mixed with each other. The "quasiparticle structures" of the yrast and yrare bands for the eight-particle system are given in Tables III and IV. Considering the selection rules for the Coriolis

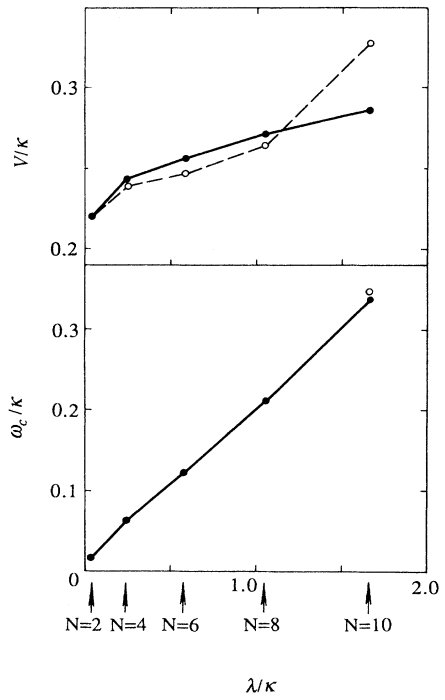

FIG. 2. The variations of the yrast-yrare interaction V and the bandcrossing frequency ω_c with the Fermi energy λ in the single-j model. $G/\kappa=0.15$. The values from the MPC truncation ($E_c/\kappa=3.5$) and the untruncated ($E_c=\infty$) calculations are denoted by open and solid circles, respectively. The bandcrossing frequencies calculated in these two cases are almost the same except for $N=10$. This figure is taken from Ref. [21].

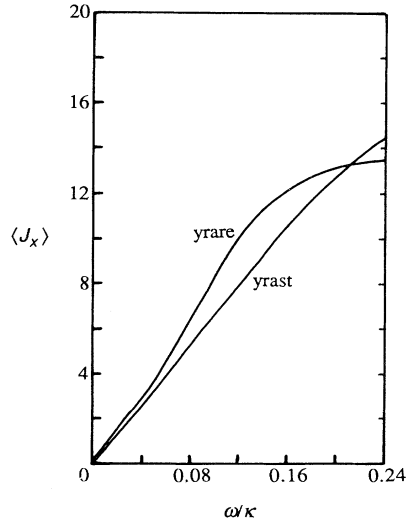

FIG. 3 $\langle J_x\rangle$ vs ω/κ plot for the yrast and yrare bands of an eight-particle system in the single-j model. $E_c/\kappa=3.5$, $G/\kappa=0.15$.

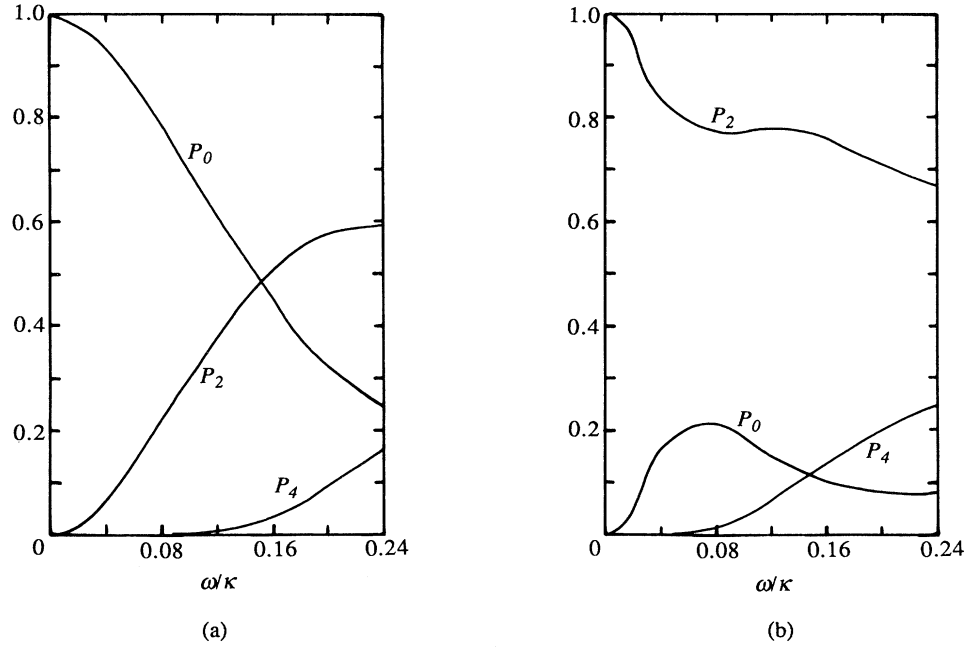

FIG. 4. The ω variation of the seniority structure for an eight-particle system in the single-j model. $E_c/\kappa=3.5$. $G/\kappa=0.15$. P_v denotes the component of seniority v configurations. (a) The yrast band. (b) The yrare band.

interaction,

Δr: no ,

$\Delta\pi$: no ,

$\Delta K=\pm 1$,

$\Delta v=0,\pm 2$,

the pair-broken $v=2$, $K^\pi=1^+$ eigenstates of H_{intr}, first of all, are gradually mixed into the yrast band. Particularly, the lowest pair-broken eigenstate $(\bar{4}5)1_1^+$ [note: its main component (weight $\geq 10\%$) is configuration $123(\bar{4}5)$] is strongly mixed into the yrast state (whose main components are configurations 1234, 1235, and 1245), hence, a spin alignment appears. In the low-ω region, the lowest (yrast) eigenstate of H_{CSM} is mainly composed of the lowest 0_1^+ states and $(\bar{4}5)1_1^+$ state of H_{intr} (see Table III).

TABLE III. The "quasiparticle structure" of the yrast and the yrare bands of H_{CSM} for an eight-particle system in the single-j model ($j=\frac{13}{2}$). The eigenstates of H_{intr}, which constitute the main components (weight $\geq 10^{-2}$) of the yrast and yrare bands of H_{CSM}, and the corresponding eigenenergies are listed in columns 1 and 2. The weights of these eigenstates in the yrast band are given in column 3 ($\omega/\kappa=0.04$) and columns 5 ($\omega/\kappa=0.08$). The similar results for the yrare band are shown in column 4 ($\omega/\kappa=0.04$) and column 6 ($\omega/\kappa=0.08$).

Eigenstates of H_{intr} $(\nu_1\nu_2)K^\pi$	Eigenenergies (in units of κ)	Weights in H_{CSM} eigenstates $\omega/\kappa=0.04$ Yrast	$\omega/\kappa=0.04$ Yrare	$\omega/\kappa=0.08$ Yrast	$\omega/\kappa=0.08$ Yrare
0_1^+	0.0000	0.9356	0.0544	0.7658	0.0882
0_2^+	1.0460		0.1081	0.0181	0.1222
$(\bar{4}5)1_1^+$	0.7368	0.0584	0.6523	0.1772	0.0880
$(\bar{3}4)1_1^+$	1.5879			0.0116	0.0470
$(\bar{5}6)1_1^+$	1.7729				0.0123
$(\bar{3}5)2_1^+$	1.1035		0.0881	0.0115	0.0951
$(\bar{4}6)2_1^+$	1.3350		0.0189		0.0169
$(\bar{2}5)3_1^+$	1.3497				0.0261
$(\bar{3}6)3_1^+$	1.7067				0.0113
$(25)6_1^+$	1.3497				0.0275
$(35)7_1^+$	1.1035				0.1215
$(45)8_1^+$	0.7368		0.0491		0.2429
$(36)8_1^+$	1.7067				0.0126
$(46)9_1^+$	1.3350				0.0252

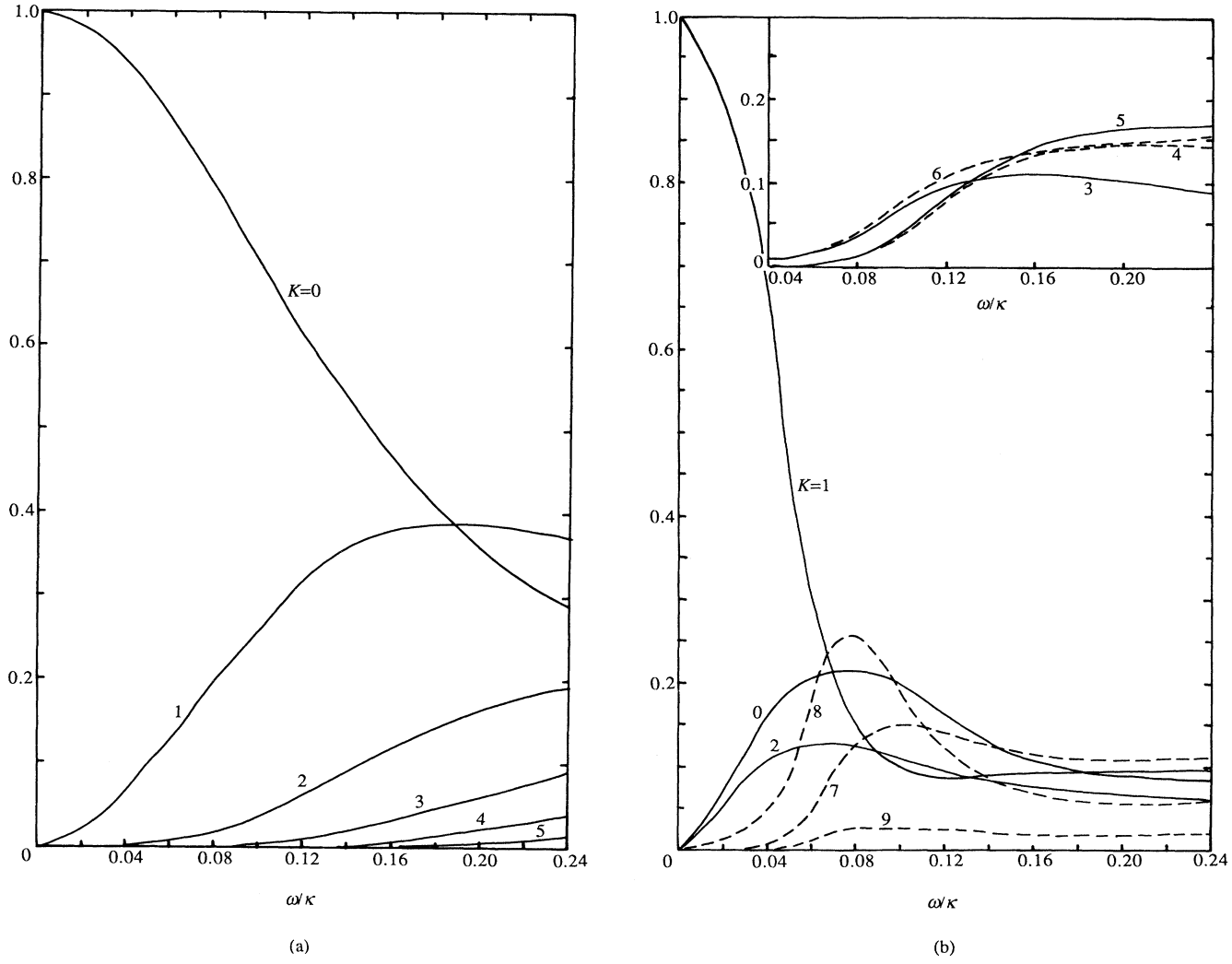

FIG. 5. The ω variation of the K structure for an eight-particle system in the single-j model. $E_c/\kappa=3.5$, $G/\kappa=0.15$. (a) The yrast band. (b) The yrare band. For clarity some small components ($K=3$, 4, 5, and 6) are plotted in the upper right inset.

With increasing ω, higher $K^\pi=1^+$ states, $K^\pi=2^+$ and higher $K^\pi=0^+$ states (through second-order perturbation), $K^\pi=3^+$ states (through third-order perturbation), etc., are successively mixed into the yrast band. For example, when $\omega/\kappa=0.08$ ($\hbar\omega\sim240$ keV) the main components of the yrast band are 0_1^+, 0_2^+, and $(\bar{4}5)1_1^+$, $(\bar{3}4)1_1^+$, and $(\bar{3}5)2_1^+$ (see Table III). However, even for a very large value of ω, e.g., $\omega/\kappa=0.20$ ($\hbar\omega\sim600$ keV), the yrast band is mainly composed of $K^\pi=0^+$, 1^+, 2^+, and 3^+ components, and those with $K>5$ are still extremely insignificant [see Table IV, also Fig. 5(a)].

From the discussion above, it is seen that in the single-j ($j=\frac{13}{3}$) model there exists no such yrast band which has no (or only a weak) response to the Coriolis interaction. As a result of the Coriolis interaction, the seniority structure and K structure of the yrast band become more and more complicated.

The situation is different for the excited bands. Because of the dense distribution of the excited eigenstates of H_{intr} [see Fig. 6(b)], the excited bands are strongly mixed with each other under the influence of the Coriolis interaction. The intrinsic structure of the excited bands of H_{CSM} often changes rapidly and their K structure becomes rather complicated even for not too high ω. For example, the lowest excited eigenstate of H_{intr}, $(\bar{4}5)1_1^+$, is strongly mixed with its neighboring eigenstates 0_2^+, $(\bar{3}5)2_1^+$, $(\bar{4}5)2_1^+$, as well as its degenerate state $(45)8_1^+$. When $\omega/\kappa=0.04$, the main components of the first excited (yrare) state of H_{CSM} are (see Table III)

$(\bar{4}5)1_1^+$ (65.23%), 0_2^+ (10.81%), $(\bar{3}5)2_1^+$ (8.81%), 0_1^+ (5.44)%, $(45)8_1^+$ (4.91%), $(\bar{4}6)2_1^+$ (1.89%).

For the yrare band in low-ω region, the superposition of the low-lying eigenstates of H_{intr} is coherent and the spin alignment $\langle J_x \rangle_{\text{yrare}}$ is, in general, larger than $\langle J_x \rangle_{\text{yrast}}$ (see Fig. 3). As the cranking frequency ω increases higher and higher, the K structure of the excited bands of H_{CSM} becomes extremely complicated and changes beyond recognition [see Fig. 5(b)]. In this case, the excited bands of H_{CSM} become superpositions of many low-lying eigenstates of H_{intr} (see Tables III and IV), among which none of them is dominant.

Due to the coherent superposition, the spin alignment of the yrast band, $\langle J_x \rangle_{\text{yrast}}$, increases step by step with increasing ω. For the yrare band, on the contrary, with increasing ω, the rising pace of $\langle J_x \rangle_{\text{yrare}}$ begins to slow down due to the destructive interference. When ω reaches a certain critical value, ω_c, the first bandcrossing occurs. However, calculation in the single-j model shows that, no abrupt exchange of features between the yrast and yrare bands occurs around $\omega \sim \omega_c$, i.e., no sharp bandcrossing or weak yrast-yrare interaction is found.

For a given N system, the distribution and property of the low-lying eigenspectra of H_{intr} determine the magni-

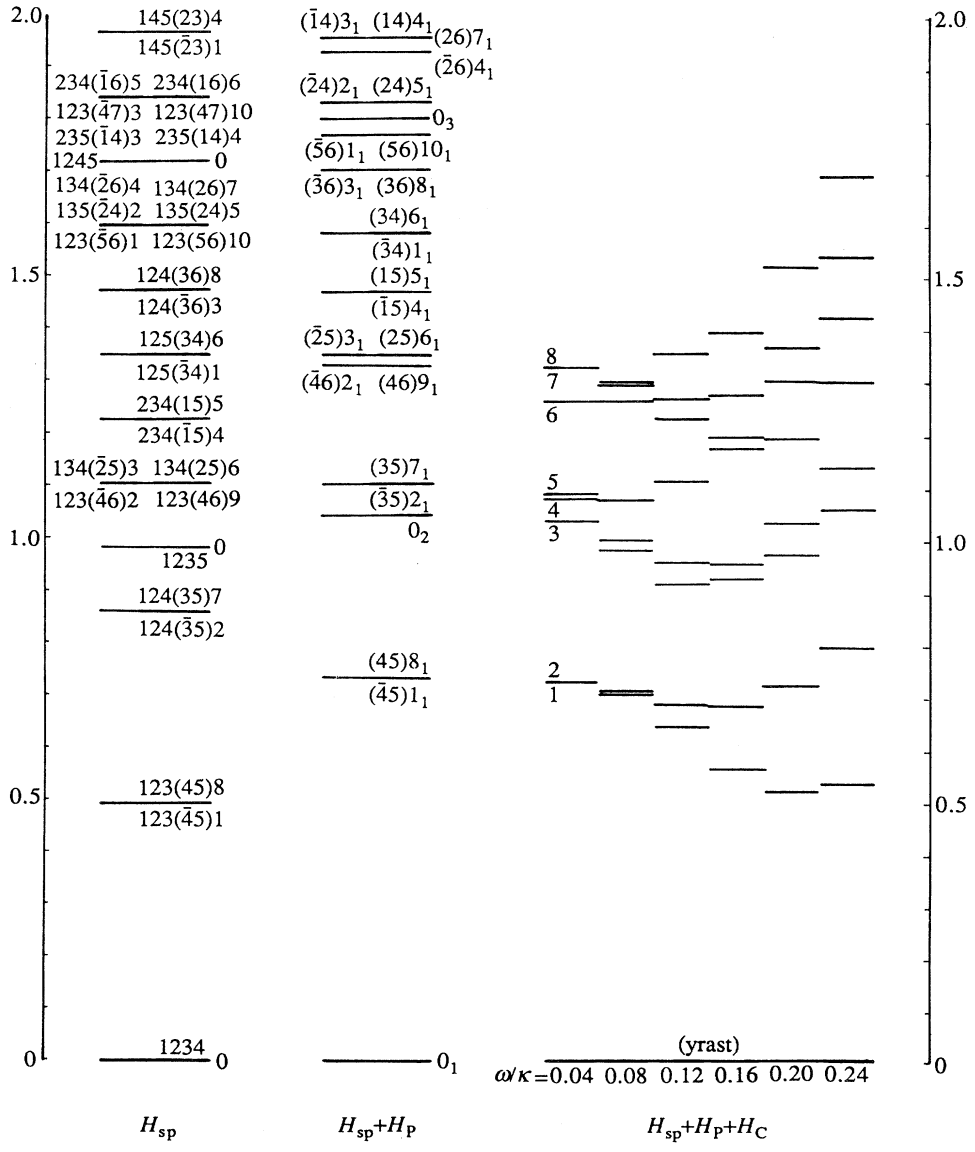

FIG. 6. The distribution of the low-lying configurations (left portion) and the low-lying eigenspectrum of $H_{\text{intr}} = H_{sp} + H_P$ (middle portion) for an either-particle system in the single-j model. $E_c/\kappa = 3.5$, $G/\kappa = 0.15$. The nine lowest eigenstates of H_{CSM} for $\omega/\kappa = 0.04$, 0.08, 0.12, 0.16, and 0.20 are shown in the right portion. Energies are in units of κ. For the notation of the configurations and the eigenstates of H_{intr}, see text.

TABLE IV. The same as Table III but for $\omega/\kappa=0.20$.

Eigenstates of H_{intr} $(\nu_1\nu_2)K^\pi$	Eigenenergies (in units of κ)	Weights in H_{CSM} eigenstates Yrast	Yrare
0_1^+	0.0000	0.1972	0.0648
0_2^+	1.0460	0.1154	
0_3^+	1.0829	0.0156	
$(\bar{4}5)1_1^+$	0.7368	0.1528	0.0638
$(\bar{3}4)1_1^+$	1.5879	0.1125	
$(\bar{5}6)1_1^+$	1.7729	0.0615	
$(\bar{5}6)1_2^+$	2.5689	0.0113	
$(\bar{2}3)1_1^+$	2.2033	0.0292	0.0116
$(\bar{3}5)2_1^+$	1.1035	0.0575	
$(\bar{4}6)2_1^+$	1.3350	0.0207	
$(\bar{2}4)2_1^+$	1.8341	0.0323	0.0170
$(\bar{1}3)2_1^+$	2.3264		0.0185
$(\bar{2}5)3_1^+$	1.3497	0.0168	
$(\bar{3}6)3_1^+$	1.7067	0.0190	
$(\bar{1}4)3_1^+$	1.9572		0.0420
$(13)3_1^+$	2.3264		0.0185
$(\bar{1}5)4_1^+$	1.4728		0.0311
$(14)4_1^+$	1.9572		0.0553
$(\bar{2}6)4_1^+$	1.9362		0.0101
$(15)5_1^+$	1.4728		0.0484
$(24)5_1^+$	1.8341		0.0500
$(\bar{1}6)5_1^+$	2.0759		0.0234
$(25)6_1^+$	1.3497		0.0552
$(34)6_1^+$	1.5879		0.0219
$(16)6_1^+$	2.0759		0.0342

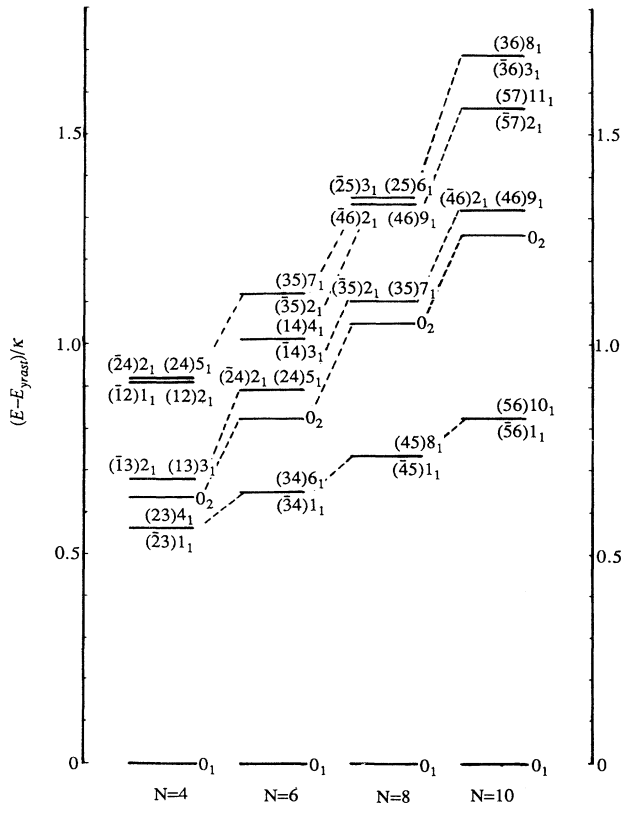

FIG. 7. Comparison of the low-lying eigenspectra of H_{intr} for $N=4$, 6, 8, and 10 particle systems. $E_c/\kappa=3.5$, $G/\kappa=0.15$.

tude of yrast-yrare interaction and the first bandcrossing frequency. The lowest nine eigenstates of H_{intr} for $N=4$, 6, 8, and 10 particle systems are displayed in Fig. 7. From the distribution of these low-lying eigenstates it is easy to understand why the first bandcrossing frequency and the yrast-yrare interaction increase monotonically with the degree of shell filling.

From the discussion above, we can see that there exist significant differences between the results about the yrast-yrare interaction obtained by using the PNC treatment for a single-j model and those by the HFB approximation. In the HFB calculation for a single-j model [1,3], it is found that the yrast-yrare interaction V is a periodic function of the Fermi energy λ which is allowed to vary continuously. When λ approaches one of the single-particle levels, V becomes very small and then a sharp backbending occurs. But when λ is situated near the middle between two adjacent single-particle levels, V reaches its maximal value. However, λ is very insensitive to the pairing interaction strength in the single-j model. Once the particle number is given in the PNC treatment, the corresponding Fermi energy λ is fixed in fact (and usually near the middle between two adjacent levels). For all even-N systems ($N=2,4,\ldots,2j-1$), the calculated V values are always rather strong. In fact, a sharp backbending implies that there exist both an yrast band (quasiparticle vacuum) which has no (or a very weak) Coriolis response and an yrare band which has a large spin alignment (a two-quasiparticle band in high-j shell). However, accurate PNC calculation in the single-j ($j=\frac{13}{2}$) model definitely shows that there exists no such

yrast band. Physically, this result can be easily understood, because all the particles occupying the high-j shell respond strongly to the Coriolis interaction. Indeed, sharp backbendings have been observed in some realistic nuclei experimentally. But we believe that the observed phenomena cannot be accounted for in the single-j model. Just for this reason, a two-j model is discussed in the next section. (See Fig. 8.)

Here we should add a few words about why the PNC result about the yrast-yrare interaction V differs so significantly from the HFB result. It is worthwhile to point out that while the PNC result is derived from the eigenfunctions of $H_{\rm CSM}$ [Eq. (1)], the HFB result is derived from the eigensolutions of $H'_{\rm CSM}=H'_{\rm intr}+H_C$ [see Eq. (5)], in which the two-body pairing interaction $H_P=-G\mathbf{P}^\dagger\mathbf{P}$ has been replaced by a one-body pairing potential $-(\Delta/2)(\mathbf{P}^\dagger+\mathbf{P})$. In the HFB approximation, the quasiparticle residual interaction and blocking effect are completely ignored, though they are very important for low-lying eigenstates. In addition, calculation shows [9] that there exist excessive spurious states in the BCS or HFB solution. Therefore, it is not surprising that there exist large differences between our PNC result and the HFB result. Some of the HFB results are qualitatively correct (e.g., the appearance of an energy gap between the ground state and the excited states, etc.), but some of them seem unreliable. A well-known and generally recognized example is the statement about the pairing collapse.

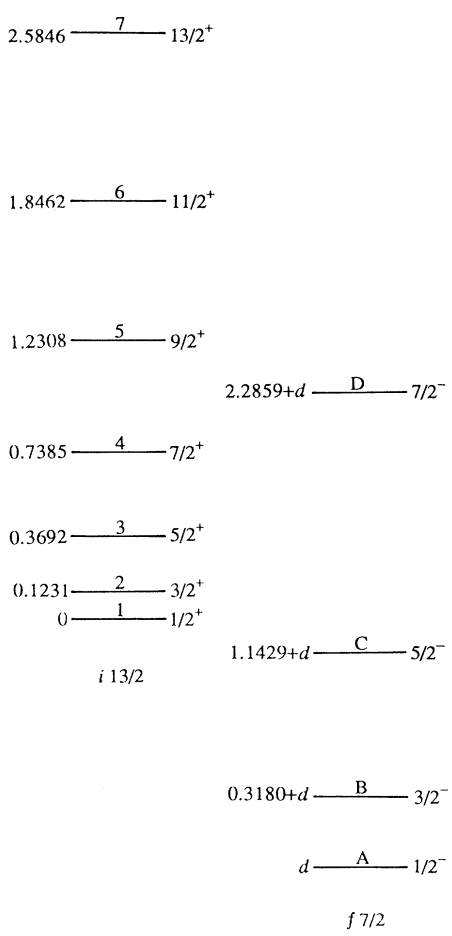

FIG. 8. The single-particle level scheme for a two-j ($i\frac{13}{2}$ plus $f\frac{7}{2}$) model (in units of k).

TABLE V. The comparison of the calculated exact results and those obtained using the MPC truncation in the single-j model ($j=\frac{13}{2}$). (a) Bandcrossing frequencies, ω_c/κ. (b) Yrast-yrare interaction strengths, V/κ.

	Exact solution	MPC truncation	
E_c/κ	∞	3.5	3.5
G/κ	0.15	0.15	Renormalized
	(a)		
$N=2$	0.0165	0.0162	0.0165
$N=4$	0.0623	0.0610	0.0629
$N=6$	0.1224	0.1230	0.1242
$N=8$	0.2112	0.2093	0.2110
$N=10$	0.3378	0.3419	0.3463
	(b)		
$N=2$	0.2202	0.2044	0.2203
$N=4$	0.2410	0.2288	0.2395
$N=6$	0.2553	0.2404	0.2469
$N=8$	0.2710	0.2585	0.2632
$N=10$	0.2858	0.3225	0.3281

It seems necessary to discuss the reliability of the MPC truncation calculation in some detail. As mentioned above, the calculation in the full (untruncated) MPC space has been also carried out, indicating that the solutions obtained in the MPC truncation are accurate enough. The calculated exact results and the comparison with those obtained using the MPC truncation are presented in Table V. It can be seen that the MPC truncation with $E_c/\kappa=3.5$ is a good approximation to the exact solutions except for $N=10$. When G/κ is fixed to be 0.15 both in the truncated calculation and in the exact calculation, we get almost the same values for bandcrossing frequencies, and slightly different values for the yrast-yrare interaction strengths. An improved result can be obtained if a renormalized G value is assumed. Obviously, as the Fermi surface rises upwards near the top of the $i\frac{13}{2}$ shell, the MPC energies spread wider, hence the degree of accuracy of the MPC truncation becomes lower provided a constant E_c is assumed. This is clearly displayed in Table V(b). For $N=2$ and 4 very accurate V values are obtained with renormalized G, and for $N=8$ the deviation of calculated V in the truncated calculation from the untruncated one is about 4%. Indeed, the truncated result somewhat differs from the exact one for $N=10$. However, even in this case, the conclusion about the strong yrast-yrare interaction still remains valid.

III. CALCULATION IN A TWO-j MODEL

Obviously, the single-j model is too simplified to account for the sharp backbending phenomena observed in

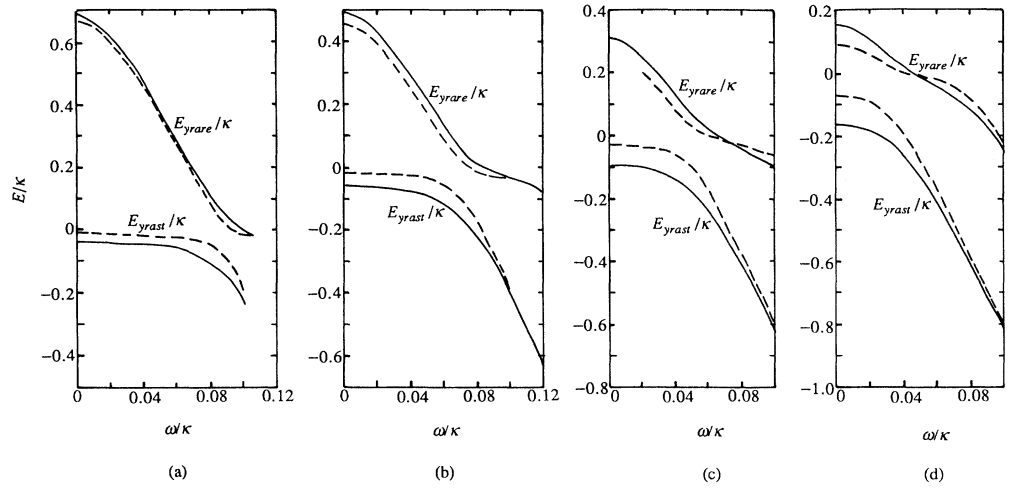

FIG. 9. E_{yrast}/κ and E_{yrare}/κ vs ω/κ plots for a six-particle system in the two-j model. $E_c/\kappa=2.0$, $G/\kappa=0.10$. Solid lines are the calculated results for constant pairing interaction and dashed lines for a modified pairing interaction (see text). The constant E_0-3G is chosen as zero in the plot, where E_0 is the energy of the lowest configuration. (a) $d=-1.5$, (b) $d=-1.4$, (c) $d=-1.3$, (d) $d=-1.2$.

some realistic nuclei. In fact, apart from the high-j intruder orbits which respond strongly to the Coriolis interaction, in the vicinity of the Fermi surface of a realistic nucleus there always exist many normal orbits of opposite parity, which have a relatively weak response to the Coriolis interaction. This fact is essential for the existence of an yrast band which has a weak Coriolis response observed in realistic nuclei. As an improvement on the single-j model, calculation in a schematic two-j model (see Fig. 8) was carried out to investigate the possibility of weak yrast-yrare coupling.

In Fig. 8, as an imitation of the normal orbits of opposite parity, a set of low-j ($j^{\pi}=\frac{7}{2}^{-}$) orbits are inserted into the set of high-j ($j^{\pi}=\frac{13}{2}^{+}$) orbits. The singe-particle levels are denoted by figures 1,2, . . . , 7 for the high-j orbits, and alphabets A, B, C, and D for $|\Omega|=\frac{1}{2}$, $\frac{3}{2}$, $\frac{5}{2}$, and $\frac{7}{2}$ members of the low-j orbits. The relative separation between two sets of orbits is described by

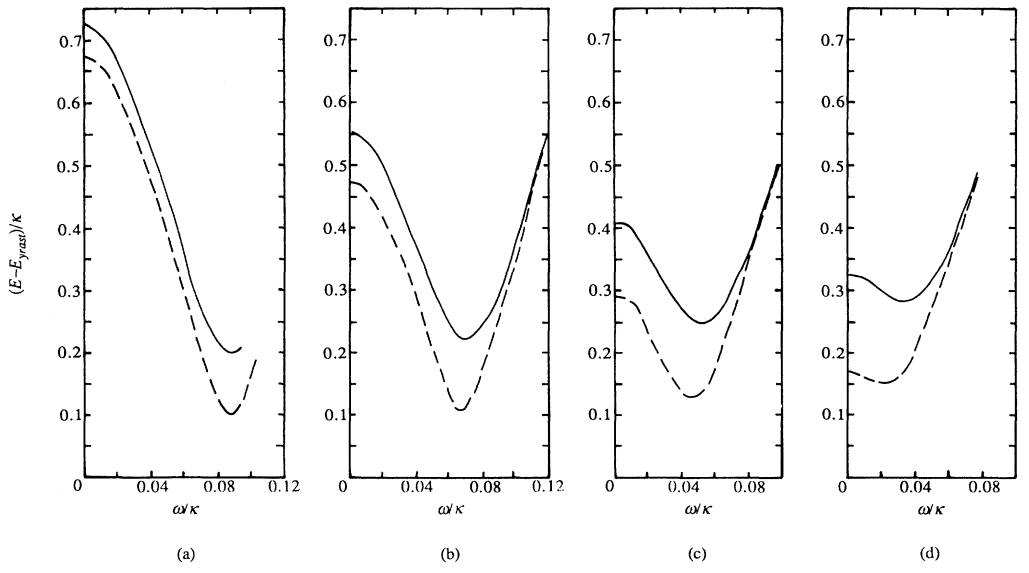

FIG. 10. The same as Fig. 9 but for $(E_{\text{yrare}}-E_{\text{yrast}})/\kappa$.

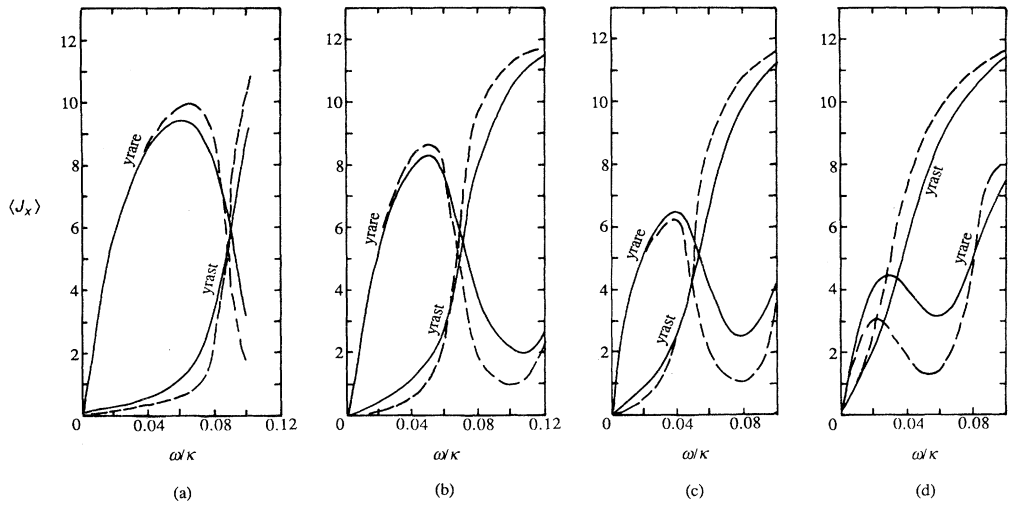

FIG. 11. The same as Fig. 9 but for the spin alignments, $\langle J_x \rangle_{\text{yrast}}$ and $\langle J_x \rangle_{\text{yrare}}$.

$$d = \varepsilon(\Omega^{\pi}=\tfrac{1}{2}^{-}) - \varepsilon(\Omega^{\pi}=\tfrac{1}{2}^{+}) \ . \tag{10}$$

For a six-particle system, the calculated results of the lowest two eigenvalues of H_{CSM}, E_{yrare}/κ and E_{yrast}/κ, and their differences are shown by solid lines in Figs. 9 and 10, respectively. The spin alignments are given in Fig. 11. The numbers of particles occupying the high-j orbits, $n_{i\,13/2}$, for the yrast and yrare bands are shown in Fig. 12. Calculations have been carried out for a series of d values. The results for $d/\kappa=-1.5$, -1.4, -1.3, and -1.2 are displayed separately in (a), (b), (c), and (d) of each figure. In the calculation we choose $E_c/\kappa=2.0$ and $G/\kappa=0.10$, which are smaller than those used in the single-j model because of the higher level density in the two-j model.

From Fig. 10 it is seen that cases (a) and (b) are close to a weak yrast-yrare interaction (sharp bandcrossing), while cases (c) and (d) are close to a strong one. This result can be understood from Figs. 9 and 11. In case (a), the yrast band has a weak response to the Coriolis interaction. For not too large values of ω (say, $\omega/\kappa<0.08$), the spin alignment of the yrast band $\langle J_x \rangle_{\text{yrast}}$, remains very small and E_{yrast} drops only a little. On the contrary, the yrare band has a strong Coriolis response, i.e., $\langle J_x \rangle_{\text{yrare}}$ rises rapidly and E_{yrare} drops down rapidly with increasing ω [see Figs. 9(a) and 11(a)]. The reason is that in the yrast band almost all the six particles stay in the normal low-j orbits A ($\Omega^{\pi}=\frac{1}{2}^{-}$), B ($\Omega^{\pi}=\frac{3}{2}^{-}$), and C ($\Omega^{\pi}=\frac{5}{2}^{-}$) which have a relatively weak response to the Coriolis interaction, while the main configurations of the yrare band is $AB1$, which has a pair of particles occupying the high-j low-Ω orbit 1 ($|\Omega|^{\pi}=\frac{1}{2}^{+}$). As ω/κ tends to 0.09, a sharp bandcrossing occurs, i.e., the yrast band and the yrare band exchange their features abruptly, which manifests in the sharp rising of $\langle J_x \rangle_{\text{yrast}}$ and $(n_{i\,13/2})_{\text{yrast}}$ as well as the sharp decreasing of $\langle J_x \rangle_{\text{yrare}}$ and $(n_{i\,13/2})_{\text{yrare}}$. The yrast band gets a spin-alignment increment of about $8\hbar$. The situation in case (d) is, however, quite different. The yrast band and the yrare band have a comparable Coriolis response [see Figs. 9(d) and 11(d)], which can be understood in terms of the particle occupation number in the high-j orbits [Fig. 12(d)].

It is worthy to note that in our treatment the total

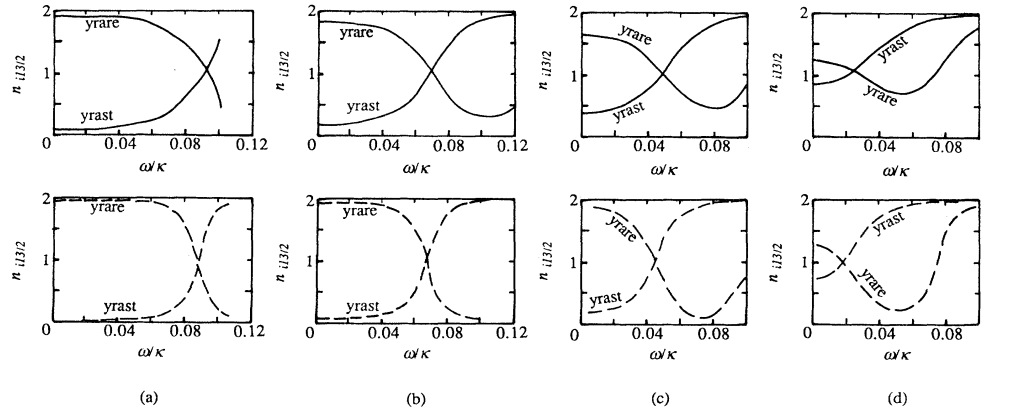

FIG. 12. The same as Fig. 9 but for the particle numbers in the $i\frac{13}{2}$ orbits, $(n_{i\,13/2})_{\text{yrast}}$ and $(n_{i\,13/2})_{\text{yrare}}$.

number of particles is conserved exactly, but the numbers of particles in the high-j orbits and in the normal orbits are not conserved separately. From Fig. 12 it is seen that $n_{i\,13/2}$ vs ω plots for the yrast and yrare bands vary smoothly in the low-ω region, and intersect with each other around the bandcrossing. In Fig. 12(a), the particle numbers in the high-j orbits, $(n_{i\,13/2})_{\text{yrast}}$ and $(n_{i\,13/2})_{\text{yrare}}$, are significantly different and an abrupt change occurs near bandcrossing, which implies a sharp bandcrossing. On the contrary, in Fig. 12(d), the values of $n_{i\,13/2}$ for these two bands are comparable, therefore, only a slightly exchange of their features occurs in the bandcrossing region. This result reminds us of the work of Ref. [7], in which the physical nature of the oscillating behavior of the yrast-yrare interaction was analyzed in a cluster-rotor weak-coupling model. In this model the whole nucleus is split into a core and a valence nucleon ($i\frac{13}{2}$) system. Exchange of nucleon pair between the core and the valence system is allowed. The total particle number is conserved in the model, but the particle numbers of both the core and the valence system are not conserved separately. It was found that the periodic disappearance of the yrast-yrare interaction can be attributed to the mixing of states with different particle numbers in the valence system. It seems that the core plays a similar role to the low-j shell in the two-j model.

Observation of Figs. 9–12 also shows that the bandcrossing frequency decreases step by step from case (a) to case (d). This fact can be easily explained in terms of the distribution of the low-lying configurations (Fig. 13), or the low-lying eigenspectrum of H_{intr} (Fig. 14). In case (a), the pair-broken configurations, which have strong Coriolis response [e.g., $AB(\bar{1}2)K^{\pi}=1^{+}$, $AB(\bar{2}3)K^{\pi}=1^{+}$, $AB(12)K^{\pi}=2^{+}$, $AB(\bar{1}3)K^{\pi}=2^{+}$, etc.] lie rather high, i.e., the energy gap is rather large, hence a higher rotational frequency for the first bandcrossing is expected. In case (d), the relevant configurations lie rather low [see Fig. 13(d)], i.e., the energy gap is rather small, so the yrast-yrare bandcrossing occurs even for rather low-ω values.

Up to now, we have assumed that the pairing interaction strength G is the same for all the pair transitions [14] i.e., the matrix element

$$\langle \bar{\mu}\mu|H_P|\nu\bar{\nu}\rangle = -G$$

no matter what shells the initial pair and the final pair occupy. As we know, in heavy nuclei neutrons and protons fill different major shells, and pairing interaction between them is usually considered to be very weak and is neglected completely. Experience tells us such an assumption seems reasonable. Similarly, we also have tentatively assumed a modified pairing interaction, namely,

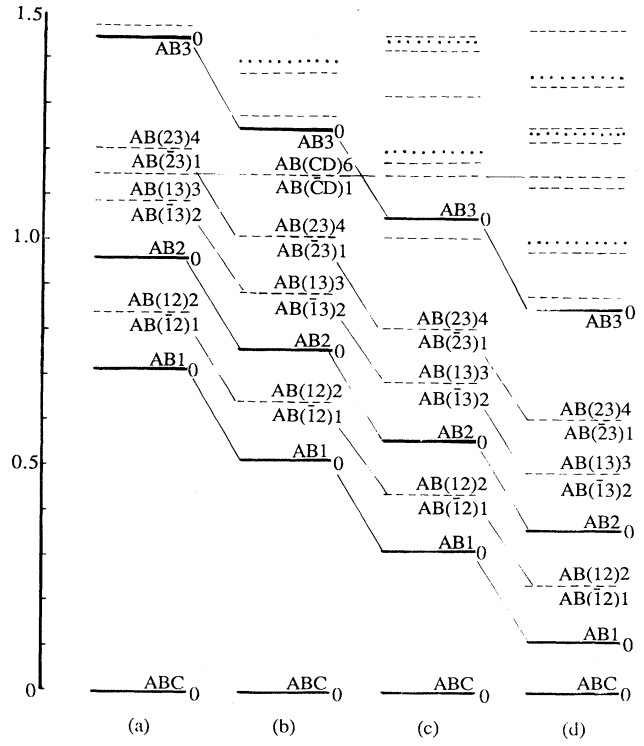

FIG. 13. The same as Fig. 9 but for the distribution of the low-lying configurations. The configuration energies are in units of κ. The solid lines, dashed lines, and dotted lines are for the fully paired configurations, pair-broken ($v=2$) configurations, and two-pair-broken ($v=4$) configurations, respectively.

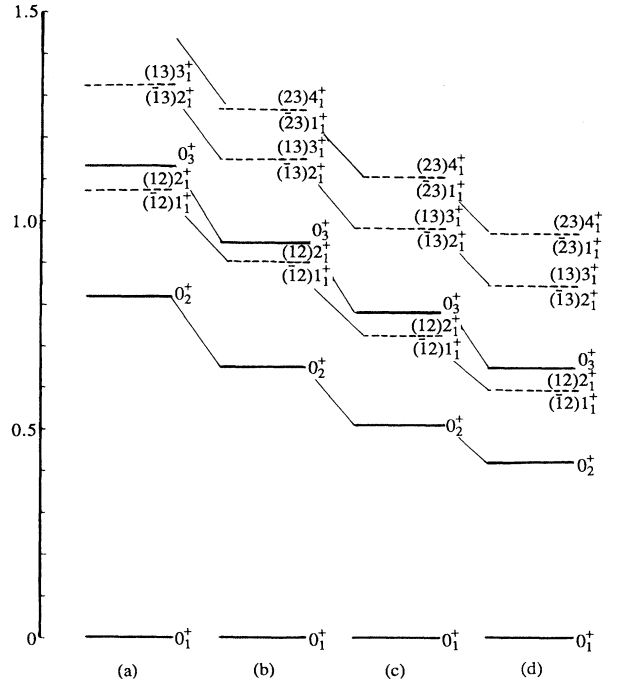

FIG. 14. The same as Fig. 9 but for the distribution of the low-lying eigenstates of H_{intr}. The eigenenergies are in units of κ. The solid lines and dashed lines are for the pair-excitation states ($v=0$, $K^{\pi}=0^{+}$) and pair-broken states ($v=2$), respectively.

$$\langle \bar{\mu}\mu | H_P | \nu\bar{\nu} \rangle = \begin{cases} -G, & \text{if states } \mu \text{ and } \nu \text{ belong to the same oscillator major shell ,} \\ -\frac{1}{2}G, & \text{if the single-particle states } \mu \text{ and } \nu \text{ belong to different oscillator major shells .} \end{cases}$$

For comparison the corresponding calculated results are also given in Figs. 9–12 by the dashed lines. It is interesting to see that the modified pairing interaction leads to a weaker yrast-yrare interaction than that for a constant pairing interaction.

IV. SUMMARY

In the present paper the yrast-yrare interaction strength and bandcrossing frequency are investigated using the PNC formalism, in which a MPC truncation is adopted instead of the usual SPL truncation. The accurate calculation in a single-j model shows that the yrast-yrare interaction strength V is always strong and no periodic oscillation of V with the degree of shell filling is found. Calculation definitely shows that in the single-j model there exists no such yrast band, which has no (or a very weak) Coriolis response.

Calculation in a two-j model shows that the coexistence of normal low-j orbits with high-j intruder orbits of opposite parity is absolutely indispensable for a weak yrast-yrare interaction observed in some realistic nuclei. For appropriate single-particle level distributions in the two-j model, weak yrast-yrare interactions do occur. In this case, the particle numbers in the high-j orbits for the yrast and yrare bands change abruptly near the first bandcrossing, which implies a sharp exchange of their features ($\langle J_x \rangle$, $n_{i\,13/2}$, etc.). Calculation shows that the yrast-yrare interaction strength depends sensitively on the single-particle level distribution around the Fermi surface, especially on the separation between the normal low-j shell and the high-j intruder shell. Thus, investigation of the yrast-yrare interaction and bandcrossing frequency could provide detailed information on the single-particle level distribution near the Fermi surface.

Calculation with a suitable Nilsson level scheme for realistic nuclei ($^{166-172}$Yb isotope chain) has been carried out. The results show that the observed zigzag variation of the yrast-yrare interaction with neutron number (e.g., a sharp backbending in ^{166}Yb and ^{170}Yb but no backbending in ^{168}Yb and ^{172}Yb) can be reproduced well in the PNC calculation. Details will be published elsewhere.

ACKNOWLEDGMENTS

This work was supported by the Doctoral Program Foundation of Institution of Higher Education of China and also by a grant from the Institute of Theoretical Physic of the Chinese Academy of science for the full space calculation. The authors gratefully acknowledge valuable discussions with Dr. R. Bengtsson.

*Mailing address: Department of Physics, Peking University, Beijing, 100871, China.

[1] R. Bengtsson, I. Hamamoto, and B. R. Mottelson, Phys. Lett. **73B**, 259 (1978).
[2] I. Hamamoto, Nucl. Phys. **A271**, 15 (1976).
[3] R. Bengtsson and H. B. Håkansson, Nucl. Phys. **A357**, 61 (1981).
[4] J. Almberger, I. Hamamoto, and G. Leander, Phys. Lett. **80B**, 153 (1979).
[5] C. G. Anderson and J. Krumlinde, Nucl. Phys. **A334**, 486 (1980).
[6] H. B. Håkansson, Phys. Lett. **94B**, 288 (1980).
[7] F. Grümmer, K. W. Schmid, and A. Faessler, Nucl. Phys. **A326**, 1 (1979).
[8] L. F. Canto, P. Ring, and J. O. Rasmussen, Phys. Lett. **161B**, 21 (1985).
[9] J. Y. Zeng and T. S. Cheng, Nucl. Phys. **A405**, 1 (1983).
[10] A. Goodman, Nucl. Phys. **A256**, 113 (1976).
[11] P. Ring, R. Beck, and H. J. Mang, Z. Phys. A **231**, 10 (1970).
[12] L. Edigo and P. Ring, Nucl. Phys. **A388**, 19 (1980).
[13] R. Bengtsson and J. D. Garrett, Int. Rev. Nucl. Phys. **2**, 193 (1984).
[14] S. T. Belyaev, Mat. Fys. Medd. Dan. Vid. Selsk. **31**, No. 11 (1959).
[15] S. G. Nilsson and O. Prior, Mat. Fys. Medd. Dan. Vid. Selsk. **32**, No. 16 (1961).
[16] J. Y. Zeng, T. S. Cheng, L. Cheng, and C. S. Wu, Nucl. Phys. **A411**, 49 (1983); **A414**, 253 (1984); **A421**, 125 (1984).
[17] D. J. Rowe, *Nuclear Collective Motion* (Methuen, London, 1970), p.194.
[18] C. S. Wu and J. Y. Zeng, Phys. Rev. C **40**, 998 (1989).
[19] C. S. Wu and J. Y. Zeng, Phys. Rev. C **41**, 1822 (1990).
[20] C. S. Wu and J. Y. Zeng, Phys. Rev. C **39**, 666 (1989).
[21] C. S. Wu and J. Y. Zeng, Phys. Rev. Lett. **66**, 1022 (1991).
[22] J. Y. Zeng, C. S. Wu, L. Cheng, and C. Z. Lin, Phys. Rev. **41**, 2911 (1990).